Fine-scale Airborne Doppler Radar Measurements of Vertical Air Motions within Long Lake-Axis-Parallel Lake-effect Snow Bands

Christopher J. Johnston, Jeffrey W. Frame and Robert M. Rauber

Department of Atmospheric Sciences - University of Illinois at Urbana-Champaign

Introduction

Communities near the Great Lakes are frequently inundated with significant lake-effect snowfalls each winter, which can cripple aviation, ground transportation, industry, and result in injuries, deaths, and significant damage to property (Kristovich et al. 2000). The Ontario Winter Lake-effect Systems (OWLeS) Project collected a comprehensive dataset on several lake-effect events during the winter of 2013/14.

This work examines the evolution, modes, and structure of vertical air motions within long lake-axis-parallel (LLAP) bands as they move over Lake Ontario and the adjacent topography east of the lake.

Data and Methods

15-m resolution Doppler radar data were collected by the Wyoming Cloud Radar (WCR) aboard the Wyoming King Air (WKA) aircraft within 7 LLAP bands near Lake Ontario during OWLeS. Data collected on 16 December 2013 are presented. The flight track of the WKA within the LLAP band is depicted in Fig. 1.

Contoured frequency by altitude diagrams (CFADs; Yuter and Houze 1995) reveal how the distributions of vertical radial velocity and equivalent reflectivity factor (hereafter reflectivity) measured by the WCR vary with altitude. This allows for inference of the presence of different modes of convection or microphysical processes within the LLAP bands.

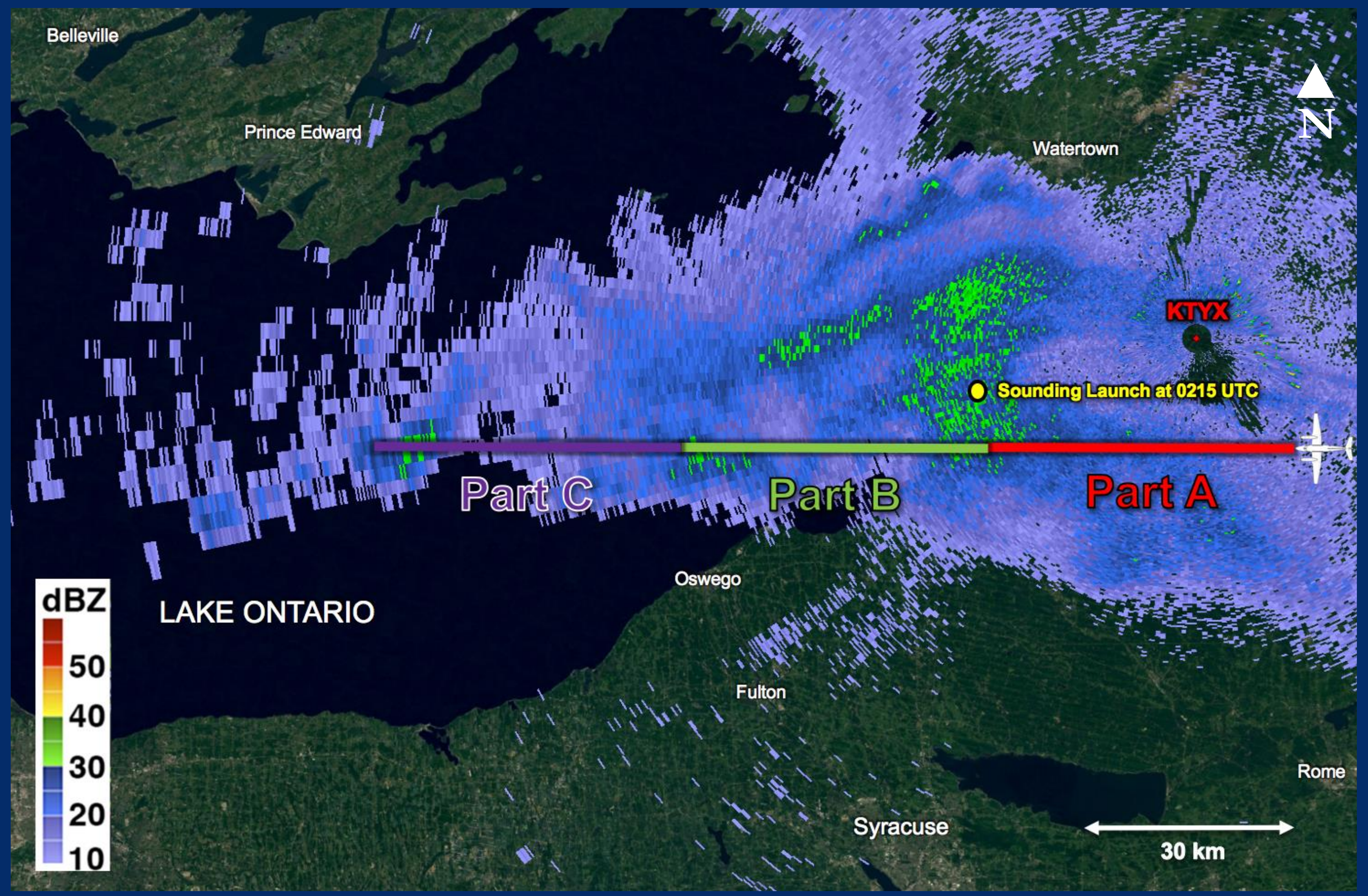

Fig. 1. Reflectivity at 0.5° from the KTYX WSR-88D at 0130 UTC 16 December 2013. WKA flight leg is shown as the colored line. Part A of leg (red line), Part B of leg (green line), and Part C of leg (purple line) are indicated. The Sandy Creek sounding launch site is signified by a yellow dot. Note: Ground clutter from wind turbines and other sources are present to the northeast of the radar site.

Wyoming Cloud Radar Data and CFADs

Over Land: Part A

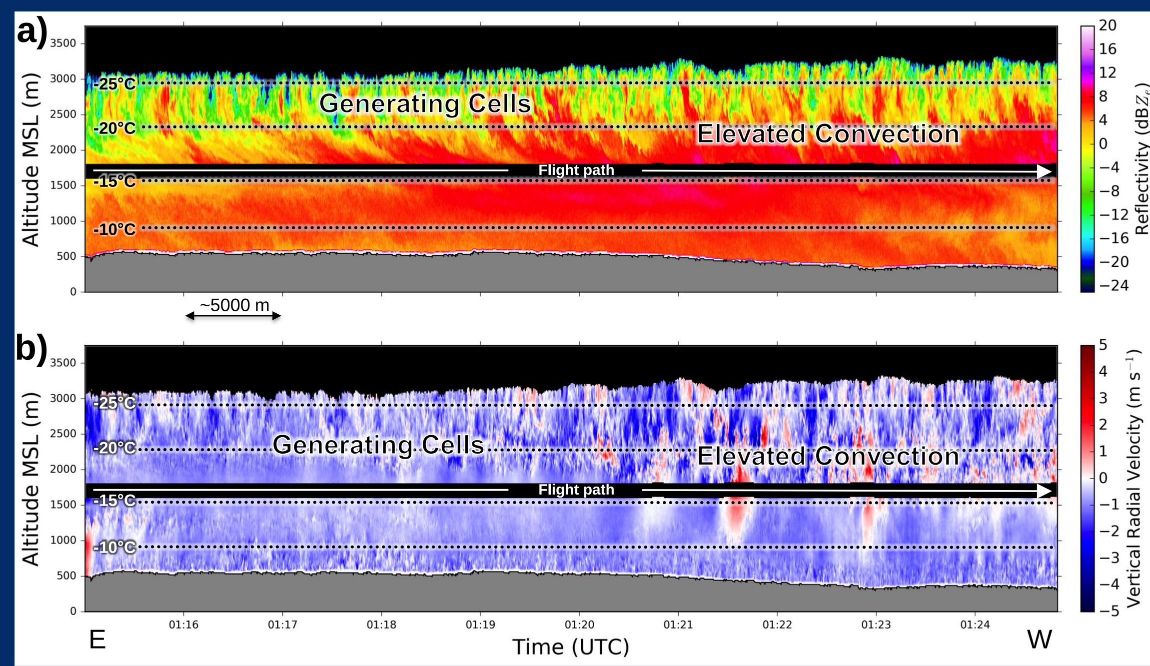

Fig. 2a. Along-band cross-section of WCR reflectivity from 0115-0125 UTC. Sounding-derived temperatures are overlaid. Flight path is shown at an altitude of ~1700 m above mean sea level (MSL). Cloud top generating cells (GCs) are ubiquitous along this leg. Higher reflectivities likely associated with elevated convection in the area of maximum dendritic growth of ice crystals (above 1500 m MSL).

Fig 2b. Along-band cross-section of WCR vertical radial velocity from 0115-0125 UTC. The updraft speeds within the GCs are on the order of 1-2 m s^{-1}, while the surrounding downdraft speeds are on the order of 1-3 m s^{-1}. Maximum updraft speeds within the elevated convective cells are ~4-5 m s^{-1}. Weak surface-based convection is also present below 1000 m MSL.

Land-to-lake Transition: Part B

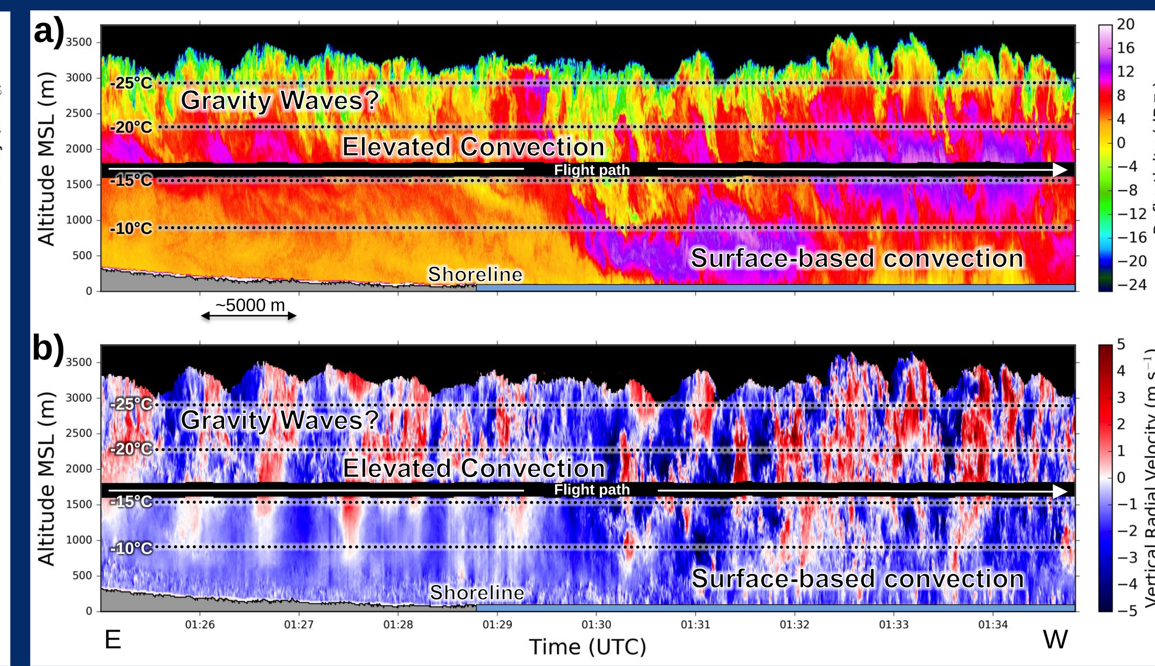

Fig. 3a. As in Fig. 2a, but for 0125-0135 UTC. Intense surface-based convection is present at all levels over the lake. One reflectivity maximum occurs at an altitude of ~1700 m MSL with significant attenuation below, likely due to supercooled water (SW) embedded within the convection. A second maximum is found just above the surface of the lake in areas without attenuation. Reflectivity increases above ~1500 m MSL over land, likely due to elevated convection or possible gravity waves above this altitude.

Fig. 3b. As in Fig. 2b, but for 0125-0135 UTC. Deep surface-based convection over the lake exhibits updrafts and downdrafts with maximum strengths between 4-6 m s^{-1}. Probable gravity waves are seen above 2000 m MSL, especially over land. The updraft and downdraft speeds inside these features are on the order of 1-3 m s^{-1}.

Over Lake: Part C

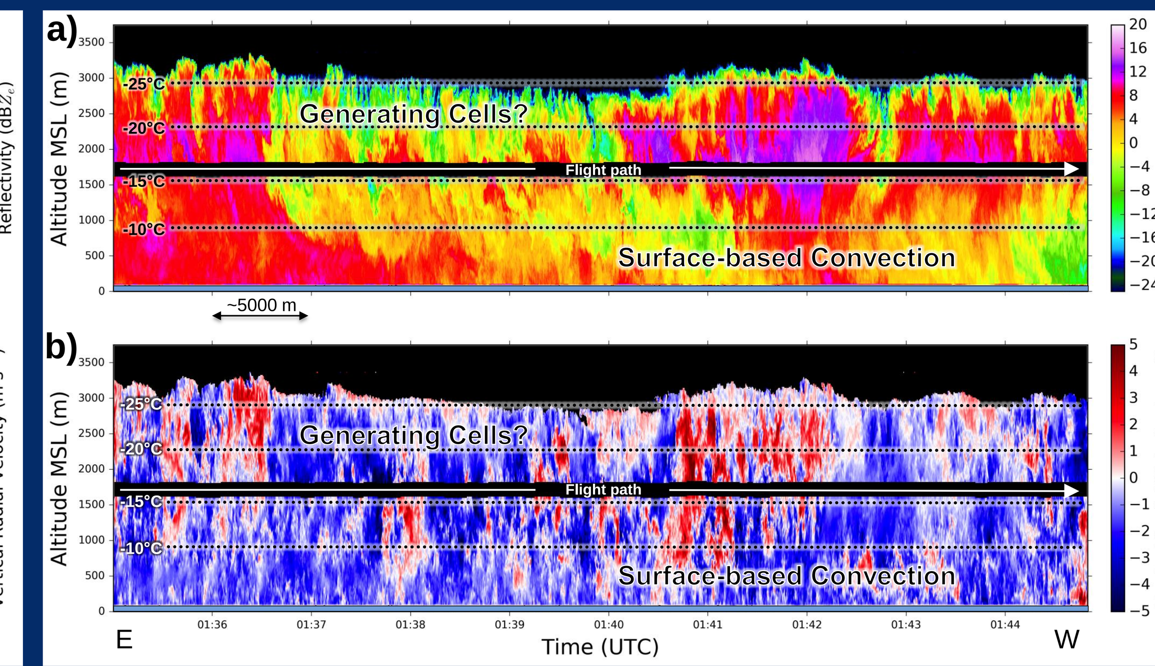

Fig. 4a. As in Fig. 2a, but for 0135-0145 UTC. Robust surface-based convection occurs throughout this leg. As in Fig. 3a, attenuation below 1500 m MSL is most likely caused by SW within the convection. Lofting of frozen hydrometeors downstream (eastward) and subsequent growth may explain the reflectivity maximum below 1000 m MSL on the eastern portion of the flight leg. Possible GCs are present in the eastern portion of the flight leg.

Fig. 4b. As in Fig. 2b, but for 0135-0145 UTC. Maximum updraft speeds of around ~6 m s^{-1} occur within the deep surface-based convective updrafts. Surface-based updrafts reach the top of the cloud. The updrafts/downdrafts within the GCs and are of the same magnitude as those in Fig. 3b.

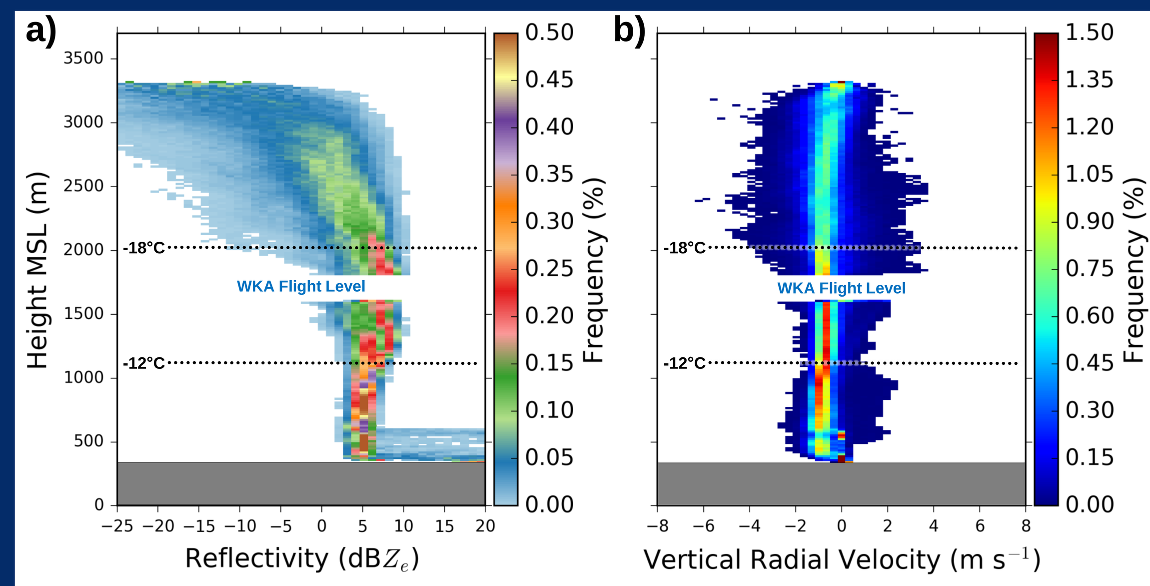

Fig. 5a. CFAD of reflectivity for Part A of the flight leg. Sounding-derived temperatures denoting the dendritic growth zone are overlaid. Dendritic growth is noted because the reflectivities increase with decreasing altitude. The large spread in reflectivity above the flight level is indicative of GCs. A more uniform reflectivity field is seen below the GC level (~2000 m MSL) which suggests a seeder-feeder process, whereby the GC seeds the stratiform cloud below. Attenuation owing to SW is likely the cause of why reflectivities decrease with decreasing altitude below 1500 m MSL.

Fig 5b. CFAD of vertical radial velocity for Part A of the flight leg. Above the flight level, a large distribution of vertical radial velocity is seen (-5 to 4 m s^{-1}) which is indicative of elevated convection and GCs. The wider distribution just above the surface is owing to the weak surface-based convection over land noted above. The mean hydrometeor fall out speed is about 1 m s^{-1}.

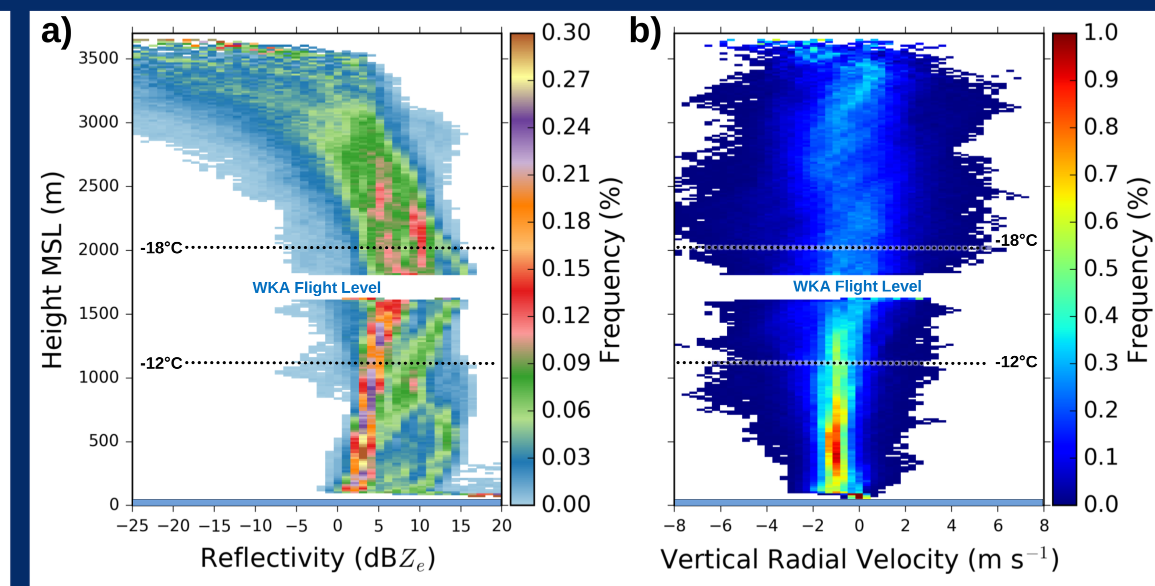

Fig. 6a. As in Fig. 5a, except for Part B of the flight leg. Rapid growth is again noted above flight level. Particle sizes have increased owing to the sampling of some of the stronger surface-based convection over the lake. Attenuation from SW is more noticeable in this case owing to more intense surface-based convection over the lake, and thus an increased concentration of SW.

Fig 6b. As in Fig. 5b, but for Part B of the flight leg. The larger distribution and the monotonic increase in the spread of the vertical velocities with altitude is a strong indicator of robust surface-based convection extending to cloud top. This signal overwhelms those of the other modes of convection seen in Part A. The uniformity in the vertical velocities near the surface is reflective of the speed of the falling hydrometeors.

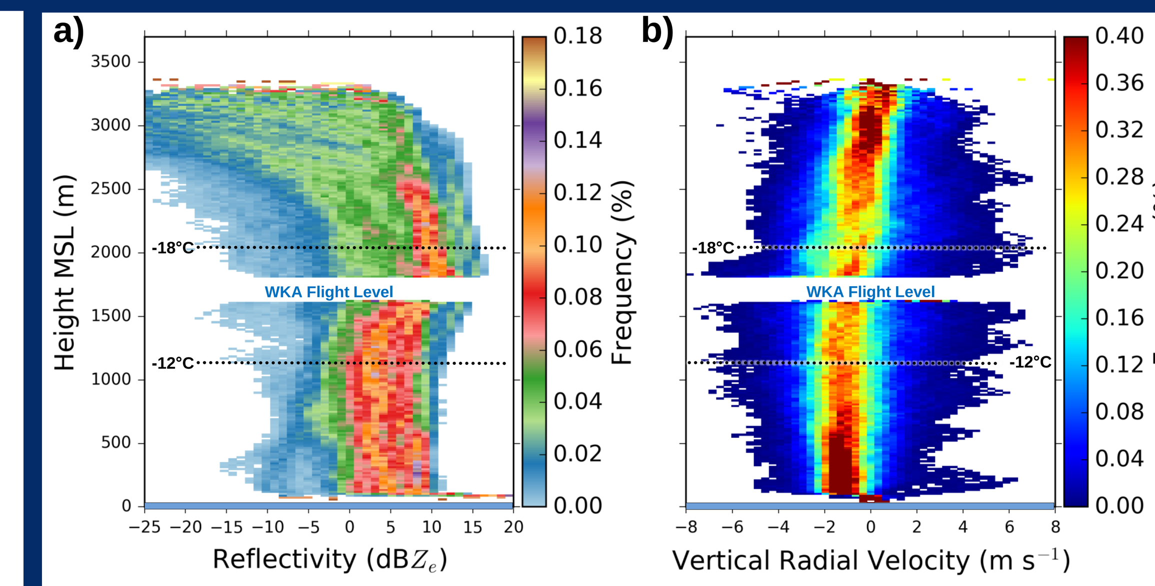

Fig. 7a. As in Fig. 5a, except for Part C of the flight leg. The particles are again of larger sizes since this leg only includes the stronger convection over the lake. The attenuation below 1800 m MSL is also worse since SW is more prevalent in convective precipitation.

Fig 7b. As in Fig. 5b, but for Part C of the flight leg. The distribution of vertical velocities with height exhibit the same pattern as in Part B, again indicating the presence of strong surface-based convection; the signatures of other modes are not apparent. The mean hydrometeor fall speed is near 0 m s^{-1} near the top of the cloud and is again near -1 m s^{-1} below 2000 m MSL, again signifying rapid growth and aggregation of the particles as they fall.

Conclusions

- Many different modes of convection are present within this LLAP band, including deep and shallow surface-based convection, elevated convection, generating cells, and possible gravity waves.
- As lake-effect convection moves inland, the surface-based convection weakens and becomes shallower and cloud top generating cells become more apparent. This is similar to the findings of Minder et al. (2015).
- Rapid growth of hydrometeors is apparent, especially above 2000 m MSL in strongly convective regimes. Other modes of convection are masked in the presence of strong surface-based convection.

Acknowledgements

We are grateful to Bart Geerts and Phillip Bergmaier at the University of Wyoming for their help with data post processing. We are also thankful for the tireless work by Nick Guy at the University of Wyoming and his development of the Airborne Weather Observations Toolkit (AWOT). Support from NSF Grant No. AGS 12-59257 is also acknowledged.

Web: publish.illinois.edu/chrisjohnston

Email: cjjhnst2@illinois.edu